

Path Loss in Reconfigurable Intelligent Surface-Enabled Channels

S.W. Ellingson, *Senior Member, IEEE*

Abstract—A reconfigurable intelligent surface (RIS) employs an array of individually-controllable elements to scatter incident signals in a desirable way; for example, to facilitate links between base stations and mobile users that would otherwise be blocked by terrain. Models used to analyze RIS-enabled links in wireless networks are commonly rudimentary; typically considering only the number of elements and omitting considerations such as the physical dimensions of the RIS and the radiation pattern and spacing of constituent elements. This paper presents a simple yet broadly-applicable physical model for the RIS-enabled channel that accounts for these factors. This model is then used to analyze the path loss of channels enabled by a reflectarray-type RIS, yielding insights into performance as a function of the size of the RIS, proximity of the RIS to the transmitter and receiver, and the criteria used to control the elements. Path loss is compared to that of a free space (i.e., no RIS) channel having equal path length, and the conditions required for path loss equal to this benchmark are identified.

Index Terms—Reconfigurable intelligent surfaces, electromagnetic propagation, path loss, antenna arrays, antenna radiation patterns, beamforming

I. INTRODUCTION

A reconfigurable intelligent surface (RIS) is a device that scatters signals in a controlled manner in order to improve path loss, fading, and/or other characteristics of a radio link; see e.g. [1] and references therein. RIS technology is expected to have a significant impact on emerging and future mobile radio communications systems; see e.g. [2]. These devices are also referred to as large intelligent surfaces (see e.g. [3]), intelligent reflecting surfaces (IRSs; see e.g. [4]), reconfigurable metasurfaces (see e.g. [5]), and by other names. RISs are most often envisioned to be some form of reflectarray, in which control consists of changing the phase and possibly magnitude of the electromagnetic field scattered by each element individually. This class of RISs is the focus of this paper.

Models used for analysis of channels employing RISs are typically rudimentary so as facilitate theoretical analysis and to make simulation tractable. The RIS-enabled channel is commonly modeled as the sum of paths from transmitter to receiver via RIS elements, as depicted in Figure 1. Each element imparts a complex gain (i.e., phase and possibly magnitude) to its associated path. Paths are presumed to exhibit path loss proportional to either $(r_{i,n} + r_{s,n})^2$, following a “specular reflection” paradigm; or $r_{i,n}^2 r_{s,n}^2$, following a “plate scattering” paradigm. Such models can be used to explore aspects of the RIS-enabled channel that do not depend critically on the

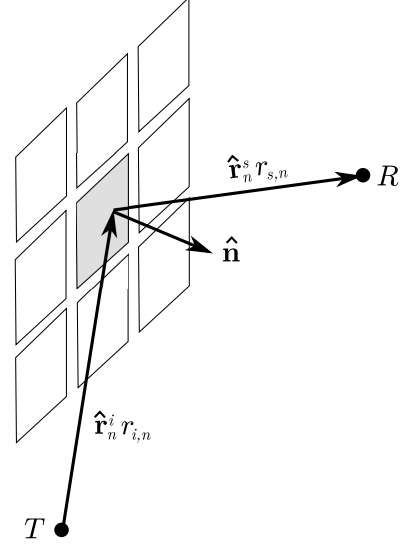


Fig. 1. Geometry for scattering from element n of an N -element RIS. The transmitter and receiver are indicated as T and R respectively. The unit vectors \hat{r}_n^i and \hat{r}_n^s are used to indicate directions from the transmitter (“incident”) and to the receiver (“scattered”), respectively. The unit vector \hat{n} indicates the outward-facing perpendicular (“broadside”) direction.

path loss of the aggregate channel. However, a few important aspects of RIS-enabled channels depend on physical behaviors that may not be captured by these models. Prominent among these aspects is the *absolute* path loss of the RIS-enabled channel, which is a principal consideration in determining the required size (i.e., physical area, number of elements, and element spacing) of the RIS. Size is of great concern due to the potentially high cost of a RIS, and the fact that this cost is expected to be approximately proportional to physical area and number of elements in the RIS. Of course, the question as to whether a RIS-enabled channel should exhibit path loss resembling specular reflection, plate scattering, or something else entirely – and under what conditions – is itself a fundamental question that may have broader implications, and therefore should be addressed.

Initial work addressing these issues is reported in [6] and [7]. In [6], RISs are analyzed using principles of physical optics, leading to the conclusion that the plate scattering paradigm is correct. In [7], RISs are modeled as arrays of passive low-gain antennas, and laboratory experiments are performed to check the predictions of the model. It is found that path loss for a RIS which is far from the transmitter and receiver seems to follow the plate scattering paradigm. Path loss for a RIS which is close to the transmitter and receiver

seems to follow the specular reflection paradigm.

As in [6] and [7], this paper presents a relatively simple yet rigorous physics-based model for RIS scattering. The principal findings of [7] are confirmed, and some additional insight is provided concerning how path loss depends on the proximity of the RIS, the size of the RIS, and the criteria (e.g., beam-forming) used to control the elements. Additional contributions in this paper include: (1) The development of a physically-motivated element radiation pattern model that is generic (i.e., appropriate for analyses that aim to be independent of RIS design details) and demonstrably well-suited as a benchmark for theoretical and simulation studies. (2) Use of the model to study path loss as a function of RIS size, leading to simple guidelines concerning the path loss of RIS-enabled channels relative to free space (non-RIS-enabled) channels of equal path length.

This paper is organized as follows: In Section II, a general expression for power transfer in the RIS-enabled single-input single output (SISO) channel is derived. In Section III, the minimum amount of simplification is applied in order to obtain an expression in the form of the Friis transmission equation, facilitating a definition of path loss that is independent of transmitter and receiver characteristics. Next, a simple, generic, and physically-valid model for the element radiation pattern model is proposed and shown to be representative of the low-gain patch-type elements normally envisioned for use in RIS arrays. The element model is designed such that the broadside effective aperture of the RIS is equal to its physical aperture – a property which is both representative of physical-realizable arrays and useful as an intuitive benchmark for RIS performance. The proposed element pattern yields an expression for path loss that is simple, generic, and consistent with electromagnetic theory.

This model is then applied to the analysis of path loss in channels consisting of a RIS. Section IV considers the “far” case, in which the distances between transmitter, RIS, and receiver are large compared to the size of the RIS. In Section V, the model of Section III is applied to the general case in which the RIS is not necessarily “far”. Findings are summarized in Section VI.

II. LINK POWER EQUATION FOR THE RIS-ENABLED CHANNEL

Referring to Figure 1, the spatial power density incident on the n^{th} element is:

$$S_n^i = P_T G_T(\hat{\mathbf{r}}_n^i) \frac{1}{4\pi r_{i,n}^2} \quad (1)$$

where P_T is the total power applied by the transmitter to the transmit antenna system, $G_T(\hat{\mathbf{r}}_n^i)$ is the gain of the transmit antenna system in the direction $\hat{\mathbf{r}}_n^i$, and $r_{i,n}$ is the distance from the transmitter to the n^{th} element. The power captured by the n^{th} element is

$$P_n^i = S_n^i A_e(-\hat{\mathbf{r}}_n^i) \quad (2)$$

where $A_e(-\hat{\mathbf{r}}_n^i)$ is the effective aperture of the element in the direction of the transmitter. This effective aperture is related to the gain $G_e(-\hat{\mathbf{r}}_n^i)$ of the element as follows:

$$A_e(-\hat{\mathbf{r}}_n^i) = \frac{\lambda^2}{4\pi} G_e(-\hat{\mathbf{r}}_n^i) \quad (3)$$

where λ is wavelength. Thus:

$$P_n^i = P_T G_T(\hat{\mathbf{r}}_n^i) G_e(-\hat{\mathbf{r}}_n^i) \left(\frac{\lambda}{4\pi r_{i,n}} \right)^2 \quad (4)$$

The power density at the receiver due to scattering from the n^{th} element is:

$$S_n^s = P_n^s G_e(\hat{\mathbf{r}}_n^s) \frac{1}{4\pi r_{s,n}^2} \quad (5)$$

where P_n^s is the power applied by the RIS to the element, $\hat{\mathbf{r}}_n^s$ is the direction from the element to the receiver, and $r_{s,n}$ is the distance from the element to the receiver. The power captured by the receiver from this element is

$$P_{R,n} = S_n^s \left[\frac{\lambda^2}{4\pi} G_R(-\hat{\mathbf{r}}_n^s) \right] \quad (6)$$

where $G_R(-\hat{\mathbf{r}}_n^s)$ is the gain of the receiver’s antenna system in the direction of the element.

The efficiency ϵ_p is defined as the ratio of power applied to an element by the RIS (i.e., RIS transmitted) to the power captured by the same element (i.e., RIS received):

$$\epsilon_p = \frac{P_n^s}{P_n^i} \quad (7)$$

This factor accounts for the limited efficiency of practical antenna elements and insertion losses associated with components required to implement the desired change in magnitude and phase. If the RIS is passive, $\epsilon_p \leq 1$.

Combining expressions, we obtain:

$$P_{R,n} = P_T G_T(\hat{\mathbf{r}}_n^i) G_R(-\hat{\mathbf{r}}_n^s) \left(\frac{\lambda}{4\pi} \right)^4 \frac{G_e(-\hat{\mathbf{r}}_n^i) G_e(\hat{\mathbf{r}}_n^s)}{r_{i,n}^2 r_{s,n}^2} \epsilon_p \quad (8)$$

Already it is apparent that individual paths follow the plate scattering paradigm for path loss; i.e., each path exhibits path loss proportional to $r_{i,n}^2 r_{s,n}^2$, and this is true regardless of how magnitude or phase are manipulated at the element. The voltage-like signal observed by the receiver is:

$$y = \sum_{n=1}^N b_n \sqrt{P_{R,n}} e^{j\phi_n} \quad (9)$$

where

$$\phi_n = 2\pi \frac{r_{i,n} + r_{s,n}}{\lambda} \quad (10)$$

is the phase accrued by propagation over the path that includes the n^{th} element, and the b_n ’s are complex-valued coefficients representing the controlled responses of the elements. The power P_R observed at the receiver is maximized by setting the phase of b_n equal to $-\phi_n$, which corresponds to coherent combining of the signals arriving along the N paths at the receiver. However this of course is not the only option.

Finally, the total power P_R observed by the receiver, keeping b_n 's undetermined for now, is:

$$P_R = \left| \sum_{n=1}^N b_n \sqrt{P_{R,n}} e^{j\phi_n} \right|^2 \quad (11)$$

III. SIMPLE GENERIC MODELS FOR PATH LOSS AND ELEMENT RADIATION PATTERN

A. Path Loss Model

It is often desirable to separate factors associated with the propagation channel (including the RIS) – collectively referred to as *path loss* – from the antenna gains of the transmitter and receiver. To accomplish this, we make the following approximations: (1) $G_T(\hat{\mathbf{r}}_n^i)$ is constant with respect to n ; i.e., the gain of the transmitter is constant over the RIS. (2) $G_R(-\hat{\mathbf{r}}_n^s)$ is constant with respect to n ; i.e., the gain of the receiver is constant over the RIS. These approximations allow $G_T(\hat{\mathbf{r}}_n^i)$ and $G_R(-\hat{\mathbf{r}}_n^s)$ to be extracted from the sum in Equation 11, yielding:

$$P_R = P_T G_T G_R \left(\frac{\lambda}{4\pi} \right)^4 \cdot \left| \sum_{n=1}^N b_n \sqrt{\frac{G_e(-\hat{\mathbf{r}}_n^i) G_e(\hat{\mathbf{r}}_n^s)}{r_{i,n}^2 r_{s,n}^2}} e^{j\phi_n} \right|^2 \epsilon_p \quad (12)$$

This expression is exact if the transmit and receive antenna systems exhibit isotropic gain. However, the approximation is broadly applicable. In particular, this approximation is suitable for transmit and receive antenna radiation patterns which are only weakly directional, as is often the case for mobile devices. This approximation is also suitable for transmit and receive antenna systems exhibiting approximately constant gain over the range of directions corresponding to the RIS – this is possible even if the transmit and receive antenna systems form narrow beams, as long as the RIS is sufficiently far away.

Equation 12 is in the form of the Friis transmission equation; therefore the path loss L_{RIS} is given by:

$$L_{RIS}^{-1} = \left(\frac{\lambda}{4\pi} \right)^4 \left| \sum_{n=1}^N b_n \sqrt{\frac{G_e(-\hat{\mathbf{r}}_n^i) G_e(\hat{\mathbf{r}}_n^s)}{r_{i,n}^2 r_{s,n}^2}} e^{j\phi_n} \right|^2 \epsilon_p \quad (13)$$

B. Generic Element Pattern Model

Next, we seek an expression for the element radiation pattern $G_e(\cdot)$ that is simple yet broadly-applicable. Since RIS elements are commonly envisioned to be electrically-small low-gain elements above a conducting ground screen, we choose the popular model (see e.g., [8], Sec. 9.7.3):

$$G_e(\psi) = \gamma \cos^{2q}(\psi) \quad 0 \leq \psi < \pi/2 \quad (14)$$

$$= 0 \quad \pi/2 \leq \psi \leq \pi \quad (15)$$

where ψ is the angle measured from RIS broadside, q determines the gain of the element, and γ is the coefficient required to satisfy conservation of power. Power is conserved by requiring the integral of $G_e(\psi)$ over a surface enclosing the element to be equal to 4π sr. It is shown in [8] (Sec. 9.7.3) that this constraint is satisfied for

$$\gamma = 2(2q + 1) \quad (16)$$

An appropriate value of q is determined from the broadside gain $G_e(\psi = 0)$ of the element, if known. From Equations 14–16:

$$q = \frac{1}{4} G_e(\psi = 0) - \frac{1}{2} \quad (17)$$

For general studies of RIS-based wireless communications, it is awkward to choose q (hence the element gain) to correspond to a particular element design. Instead, a physically-motivated “benchmark” value of q is preferred. Such a value may be obtained by requiring $A_e(\psi = 0)$ to be equal to $(\lambda/2)^2$. Under this condition, the physical area of a RIS is equal to the the sum of the effective apertures of the elements when the elements are separated by $\lambda/2$. Invoking this criterion, we require:

$$A_e(\psi = 0) = \frac{\lambda^2}{4\pi} G_e(\psi = 0) = \left(\frac{\lambda}{2} \right)^2 \quad (18)$$

This yields $\gamma = \pi$, $q \cong 0.285$, and subsequently $G_e(\psi = 0) \cong 5$ dBi. This value is consistent with the gain of typical patch antenna elements, which range between 3 dBi and 9 dBi (see e.g. [8], Sec. 11.2). We therefore define the desired benchmark value of q to be:

$$q_0 = 0.285 \quad (\text{definition}) \quad (19)$$

At this point, it should be emphasized that this pattern model does not *require* that the elements be spaced by $\lambda/2$; however if the elements are spaced in this manner, the choice of $q = q_0$ will result in the broadside effective aperture of the RIS being equal to its physical aperture. Similarly, the choice of $q = q_0$ is not required, and in fact this parameter can be “tuned” to model other specific element designs. The recommended procedure if a different element gain is desired is to determine first the value of γ that yields the desired broadside gain, and then to solve for q using Equation 16.

In subsequent work, we shall assume that all element patterns are identical. In practice, the patterns of elements close to the center of a large RIS will be nearly symmetric and uniform, whereas the patterns of elements near the edge will exhibit some degree of asymmetry and gain variation [8]. Since the ratio of “edge elements” to “interior elements” is small for an electrically-large RIS, this variation will typically not significantly affect path loss calculation. Therefore, it is henceforth assumed that element patterns are identical; i.e., constant with respect to n .

C. Alternative Form of the Path Loss Equation

A useful alternative form of Equation 13 may be obtained using the element pattern model proposed in the previous section. First, note that

$$\cos \psi = \hat{\mathbf{r}}(\psi) \cdot \hat{\mathbf{n}} \quad (20)$$

where $\hat{\mathbf{r}}(\psi)$ is a unit vector pointing outward from the element, indicating the direction in which the pattern is being evaluated; $\hat{\mathbf{n}}$ is the unit normal vector indicating RIS broadside, i.e., the direction corresponding to $\psi = 0$; and “ \cdot ” denotes the scalar

(“dot”) product.¹ Now assuming the benchmark value of $q = q_0$, we find:

$$G_e(-\hat{\mathbf{r}}_n^i) = \pi (-\hat{\mathbf{r}}_n^i \cdot \hat{\mathbf{n}})^{2q_0}, \text{ and} \quad (21)$$

$$G_e(+\hat{\mathbf{r}}_n^s) = \pi (+\hat{\mathbf{r}}_n^s \cdot \hat{\mathbf{n}})^{2q_0} \quad (22)$$

Thus, Equation 13 becomes:

$$L_{RIS}^{-1} = \frac{\lambda^4}{256\pi^2} \left| \sum_{n=1}^N b_n \sqrt{\frac{(-\hat{\mathbf{r}}_n^i \cdot \hat{\mathbf{n}})^{2q_0} (+\hat{\mathbf{r}}_n^s \cdot \hat{\mathbf{n}})^{2q_0}}{r_{i,n}^2 r_{s,n}^2}} e^{j\phi_n} \right|^2 \epsilon_p \quad (23)$$

IV. FAR CASE

In this section we consider the “far” case. For the purposes of this paper, the RIS is said to be far from the transmitter if $\hat{\mathbf{r}}_n^i$ and $r_{i,n}$ are approximately independent of n ; i.e., approximately equal to the same constants $\hat{\mathbf{r}}_i$ and r_i , respectively. Similarly, the RIS is said to be far from the receiver if $\hat{\mathbf{r}}_n^s$ and $r_{s,n}$ are approximately equal to the same constants $\hat{\mathbf{r}}_s$ and r_s , respectively. No approximation is made for the phases ϕ_n : These values continue to be exact and are not assumed to be independent of n .²

A. Expressions for Path Loss in the Far Case

Under the far approximation, Equation 23 simplifies to:

$$L_{RIS}^{-1} = \frac{\lambda^4}{256\pi^2} \frac{(-\hat{\mathbf{r}}_i \cdot \hat{\mathbf{n}})^{2q_0} (+\hat{\mathbf{r}}_s \cdot \hat{\mathbf{n}})^{2q_0}}{r_i^2 r_s^2} \left| \sum_{n=1}^N b_n e^{j\phi_n} \right|^2 \epsilon_p \quad (24)$$

Equation 24 indicates that path loss in the far case is proportional to $r_i^2 r_s^2$, and therefore follows the plate scattering paradigm for path loss, regardless of the chosen coefficients (b_n 's).

Equation 24 indicates that path loss is minimized when the phase of b_n is set equal to $-\phi_n$. Assuming phase-only control of the elements, one would select $b_n = e^{-j\phi_n}$. In this case Equation 24 reduces to:

$$L_{RIS}^{-1} = \frac{\lambda^4}{256\pi^2} N^2 \frac{(-\hat{\mathbf{r}}_i \cdot \hat{\mathbf{n}})^{2q_0} (+\hat{\mathbf{r}}_s \cdot \hat{\mathbf{n}})^{2q_0}}{r_i^2 r_s^2} \epsilon_p \quad (25)$$

Recall that the benchmark element pattern proposed in Section III-B was derived from the constraint that the sum of the broadside effective apertures of the elements is equal to the physical area A of the RIS when the element spacing is equal to $\lambda/2$. If we now commit to this element spacing, then:

$$A = N \left(\frac{\lambda}{2} \right)^2 \quad (26)$$

¹The principal motivation in employing the scalar product notation is that this greatly simplifies computation. This is because $\hat{\mathbf{n}}$ is known in advance and does not change, $\hat{\mathbf{r}}$ is easy to compute, and the scalar product requires only algebraic operations. In contrast, the general expression for ψ is relatively complicated, requires trigonometric operations, and is a greater burden to compute. This additional burden can be significant when computing large amounts of performance data for a large RIS.

²Note that the concept of “far” as employed here is not necessarily equivalent to “far field” as the term is typically defined in the context of antennas and propagation (see e.g. [8]). To avoid confusion, the term “far” in this paper will refer solely to the assumed independence of distance and direction (but not path phase) with respect to n . Nevertheless, a RIS that is “far” will typically also be in the far field of the transmitter and receiver.

in which case Equation 25 can be expressed as follows:

$$L_{RIS}^{-1} = \left(\frac{A}{4\pi r_i r_s} \right)^2 (-\hat{\mathbf{r}}_i \cdot \hat{\mathbf{n}})^{2q_0} (+\hat{\mathbf{r}}_s \cdot \hat{\mathbf{n}})^{2q_0} \epsilon_p \quad (27)$$

Equation 27 indicates that path loss in the far case depends only on the physical area of the IS, and not at all on frequency. This is actually the expected result, as demonstrated in the next section.

B. Consistency with Plate Scattering Theory

Electromagnetic plate scattering theory is noted in [6] as a possible starting point for RIS scattering models. In this section it is shown that the connection to plate scattering theory is actually an *emergent* feature of RIS scattering theory, and does not need to be assumed. That is, under certain conditions the array-based model derived in previous sections yields results in which the RIS can be modeled as a passive flat plate scatterer.

To see this, imagine that an RIS in the far case is replaced by a flat perfectly-conducting plate of area A , and let us assume monostatic geometry; i.e., $\hat{\mathbf{r}}_i = -\hat{\mathbf{n}}$ and $\hat{\mathbf{r}}_s = +\hat{\mathbf{n}}$. In this case, the radar range equation (see e.g. [8], Sec. 4.6) indicates that:

$$P_R = P_T G_T G_R \frac{\lambda^2 \sigma}{(4\pi)^3 r_i^2 r_s^2} \quad (28)$$

where σ is the broadside monostatic radar cross section of the plate, which is known to be:

$$\sigma = \frac{4\pi A^2}{\lambda^2} \quad (29)$$

see e.g. [9], Sec. 3.7. Recasting Equation 28 in the form of the Friis transmission equation, the path loss L_{plate} in this scenario is given by:

$$L_{plate}^{-1} = \left(\frac{A}{4\pi r_i r_s} \right)^2 \quad (30)$$

Now note that Equation 27 gives precisely this result for $\hat{\mathbf{r}}_i = -\hat{\mathbf{n}}$, $\hat{\mathbf{r}}_s = +\hat{\mathbf{n}}$, and $\epsilon_p = 1$. Therefore Equation 27 is consistent with electromagnetic plate scattering theory.

Since the plate scattering model is both physically-rigorous and simple to compute, it serves as a useful benchmark for path loss in channels employing a RIS in the far case. However it should be noted that connection between plate scattering and RIS scattering is not universal. The equivalence demonstrated here is attributable to the use of the proposed benchmark ($q = q_0$) element pattern model with $\lambda/2$ element spacing. While various other combinations of element pattern and spacing can yield the same absolute equivalence, it is *not* true that *any* combination of element pattern and spacing will yield this equivalence. What *is* universal, however, is the $r_i^2 r_s^2$ range dependence of path loss in the far case.

C. Comparison to Specular Reflection

Specular reflection is the component of scattering from an electrically-large smooth surface which is distinct from diffraction originating from the edges of the surface. If diffraction in the direction of the receiver is negligible, then, from the

perspective of the receiver, the scattering from the surface is well-described as specular reflection. It is apparent from the previous section that the scattering from a RIS in the far case cannot be interpreted as specular reflection alone, since path loss is clearly seen to be dependent on the size of the RIS.

However, specular reflection is commonly found to be an appropriate model for scattering from terrain, buildings, and other electrically-large structures encountered in the analysis of terrestrial wireless communications systems. When this is the case, it is merely because diffraction is either negligible or not specifically of interest. This begs the question: When, if ever, is it appropriate to interpret far case RIS scattering as specular reflection? The short answer is “never,” as we shall now demonstrate. A second finding from this analysis will be a simple guideline for choosing the size of a RIS in the far case.

Consider a RIS which is oriented such that Snell’s law of reflection (i.e., angle of reflection equals angle of incidence) is satisfied at the RIS. Next, imagine that the RIS is replaced by an infinitely-large flat conducting plate which lies in the plane previously occupied by the RIS. Since the plate is infinite, there are no edges and therefore the scattering from the plate is pure specular reflection. Since the plate is flat, the phasefront curvature of the reflected wave at the point of reflection is equal to the phasefront curvature of the incident wave at the point of reflection, and the rate at which spatial power density decreases is the same after reflection as it was before reflection. Subsequently the path loss L_S in this case is simply

$$L_S = \left[\frac{4\pi (r_i + r_s)}{\lambda} \right]^2 \quad (31)$$

i.e., the path loss is equal to that of a direct (i.e., no reflection) path of length $r_i + r_s$. Subsequently the path loss for the far case RIS channel relative to that of the specular reflection channel is:

$$\frac{L_S}{L_{RIS}} = \left(\frac{r_i + r_s}{r_i r_s} \cdot \frac{A}{\lambda} \right)^2 (-\hat{\mathbf{r}}_i \cdot \hat{\mathbf{n}})^{2q_0} (+\hat{\mathbf{r}}_s \cdot \hat{\mathbf{n}})^{2q_0} \epsilon_p \quad (32)$$

Note that the ratio of the path losses is, not surprisingly, dependent on both the physical area of the RIS and frequency. However, it is also now apparent that L_S can be less than, equal to, or greater than L_{RIS} .

To better understand the situation, it is convenient to define an “effective focal length” f_e as follows:

$$\frac{1}{f_e} = \frac{1}{r_i} + \frac{1}{r_s} = \frac{r_i + r_s}{r_i r_s} \quad (33)$$

This expression is the known in the optics literature as the “thin lens equation;” however, the reason for defining f_e here is simply brevity and convenience. For example, when r_i and r_s are equal, $f_e = r_i/2 = r_s/2$. Also, when $r_i \gg r_s$, $f_e \approx r_s$; similarly when $r_i \ll r_s$, $f_e \approx r_i$. Thus, f_e generally ranges between the lesser of r_i and r_s down to about half the lesser value. Using this concept, Equation 32 simplifies to:

$$\frac{L_S}{L_{RIS}} = \left(\frac{A}{f_e \lambda} \right)^2 (-\hat{\mathbf{r}}_i \cdot \hat{\mathbf{n}})^{2q_0} (+\hat{\mathbf{r}}_s \cdot \hat{\mathbf{n}})^{2q_0} \epsilon_p \quad (34)$$

Freq.	“minimum”		“typical”	
	$f_e = 0.1$ km	1 km	$f_e = 0.1$ km	1 km
0.8 GHz	6.1 m	19.4 m	8.9 m	28.8 m
1.9 GHz	4.0 m	12.6 m	5.8 m	18.2 m
2.4 GHz	3.5 m	11.2 m	5.1 m	16.2 m
5.8 GHz	2.3 m	7.2 m	3.3 m	10.4 m
28.0 GHz	1.0 m	3.3 m	1.5 m	4.7 m
60.0 GHz	0.7 m	2.2 m	1.0 m	3.2 m

TABLE I
SIDE LENGTH OF A SQUARE RIS FOR PATH LOSS EQUAL TO THAT OF THE SPECULAR REFLECTION CHANNEL (PHYSICAL DIMENSION).

Freq.	“minimum”		“typical”	
	$f_e = 0.1$ km	1 km	$f_e = 0.1$ km	1 km
0.8 GHz	16.3 λ	51.6 λ	23.7 λ	74.8 λ
1.9 GHz	25.2 λ	79.6 λ	36.5 λ	115.3 λ
2.4 GHz	28.3 λ	89.4 λ	41.0 λ	129.6 λ
5.8 GHz	44.0 λ	139.0 λ	63.7 λ	201.5 λ
28.0 GHz	96.6 λ	305.5 λ	140.0 λ	442.7 λ
60.0 GHz	141.4 λ	447.2 λ	204.9 λ	648.0 λ

TABLE II
SIDE LENGTH OF A SQUARE RIS REQUIRED FOR PATH LOSS EQUAL TO THE SPECULAR REFLECTION CHANNEL (WAVELENGTHS).

Now we may determine the RIS size for which the path loss of these two channels is equal; i.e, $L_{RIS}/L_S = 1$. One finds:

$$A = \frac{f_e \lambda}{\sqrt{(-\hat{\mathbf{r}}_i \cdot \hat{\mathbf{n}})^{2q_0} (+\hat{\mathbf{r}}_s \cdot \hat{\mathbf{n}})^{2q_0} \epsilon_p}} \quad (35)$$

Table I shows examples of RISs meeting this criterion. Two cases are considered: “minimum,” in which $\epsilon_p = 1$ and $\hat{\mathbf{r}}_i \cdot \hat{\mathbf{n}} = 0$ (i.e., broadside incidence), yielding minimum A ; and “typical,” in which $\epsilon_p = 0.5$ and $-\hat{\mathbf{r}}_i \cdot \hat{\mathbf{n}} = \hat{\mathbf{r}}_s \cdot \hat{\mathbf{n}} = 0.5$. The “typical” case corresponds to incidence and scattering 60° off broadside with realistic efficiency, representing a practical RIS in a disadvantaged geometry. The effective focal length $f_e = 0.1$ km could be a scenario in which either r_i or r_s is ≈ 0.1 km with the other distance being much greater, $r_i = r_s = 0.2$ km, or any number of intermediate scenarios. Similarly, $f_e = 1$ km could be a scenario in which either r_i or r_s is ≈ 1 km with the other distance being much greater, $r_i = r_s = 2$ km, or any number of intermediate scenarios. Table I indicates that $L_{RIS} = L_S$ for RIS side-lengths ranging from meters to 10s of meters, depending on frequency and effective focal length.

Table II shows precisely the same result, except now expressed in electrical length; i.e, units of wavelength. Note that side-lengths ranging from $\mathcal{O}(10\lambda)$ to $\mathcal{O}(100\lambda)$ are required, as one might expect. However, additional increases in side-length do *not* yield performance comparable to specular reflection; to the contrary, the RIS outperforms specular reflection by increasing margins as the electrical size is increased. This is simply because the RIS focuses the scattered field in order to minimize path loss, whereas as the infinite conducting plate cannot.³ With this in mind, note also that a RIS could be used to accurately reproduce specular reflection, but the RIS would need to be both electrically-large *and* configured to preserve

³It is worth noting the the same result would be obtained if the RIS were replaced by a passive flat plate of equal area, but only in the monostatic broadside case since only in that case would the scattering from the plate be “focused.”

the rate of change of phasefront curvature. While this is useful in certain applications such as RIS “broadcasting,” it is not a strategy which minimizes path loss in SISO channels.

Finally, note that the *electrical* sizes of A indicated in Table II increase with frequency. In particular, note that the electrical size of A increases in proportion to $\lambda^{-1/2}$, resulting in almost an order of magnitude increase as frequency increases from 0.8 GHz to 60 GHz.

V. GENERAL CASE

When the “far” criteria defined at the beginning of Section IV are not met, one is forced to backtrack to Equation 23. In this case, the conclusions apparent in the far case do not apply and analogous conclusions for the general case are not obvious. For this reason, the following numerical study is conducted. This study assumes a planar square RIS which is again modeled as N elements with pattern $q = q_0$ which are uniformly distributed with $\lambda/2$ spacing. The transmitter is broadside to the array while the angle ψ_s to the receiver is varied from 0 (RIS broadside) to 60° and then 75° . The distances r_i and r_s are held equal and varied to generate the results shown in Figures 2, 3, and 4.

In the general case, the path loss minimization criterion $b_n = e^{-j\phi_n}$ is referred to as “focusing”. A different option is to set the phase of b_n so as to minimize path loss with respect to the directions (only) of the transmitter and receiver, which requires only that $\hat{\mathbf{r}}_i$ and $\hat{\mathbf{r}}_s$ (and not the distances r_i or r_s) be known. Specifically:

$$b_n = e^{-j(2\pi/\lambda)\mathbf{p}_n \cdot \hat{\mathbf{r}}_i} e^{+j(2\pi/\lambda)\mathbf{p}_n \cdot \hat{\mathbf{r}}_s} \quad (36)$$

where \mathbf{p}_n is the vector from a common reference point (e.g., the origin) to the location of element n . For the purposes of this paper, this is referred to as “beamforming,” and can be alternatively interpreted as collimation, or focusing at infinity. Beamforming is of practical interest, despite the non-optimum path loss, because in practice it may be easier to determine directions than positions.

The distinction between focusing and beamforming was not necessary in the far case, since under the far case approximations they are equivalent. However, when the RIS is closer, the difference in performance can be large, as we shall now see.

Figure 2 shows path gain L_{RIS}^{-1} from Equation 23, computed for $r_i = r_s = 10^4\lambda$. The result is normalized to the path gain L_S^{-1} (Equation 31) for a free space (i.e., no RIS) channel having path length $r_i + r_s$. Thus, 0 dB on the vertical axis indicates that the RIS-enabled channel exhibits path gain equal to that of the equal-length free space path. Separate curves are shown for focusing, beamforming, and the far approximation (Equation 27). The curves are too close to readily distinguish, indicating that this scenario meets the far approximation criteria. Also, note that an aperture side-length of at least 70λ is required to meet the 0 dB condition under these conditions.

Figure 3 shows the results of the same experiment performed for $r_i = r_s = 10^3\lambda$; i.e., the same RIS but one order of magnitude closer. Again, separate curves are shown

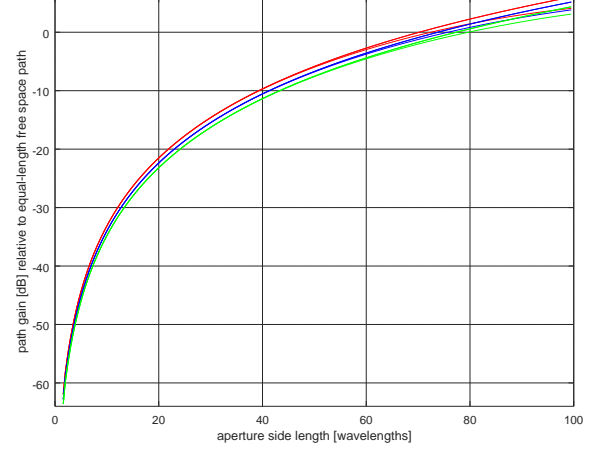


Fig. 2. Path gain relative to the equal-length free space channel for $r_i = r_s = 10^4\lambda$. Curves are shown for $\psi_s = 0^\circ$ (red), 60° (blue), and 75° (green).

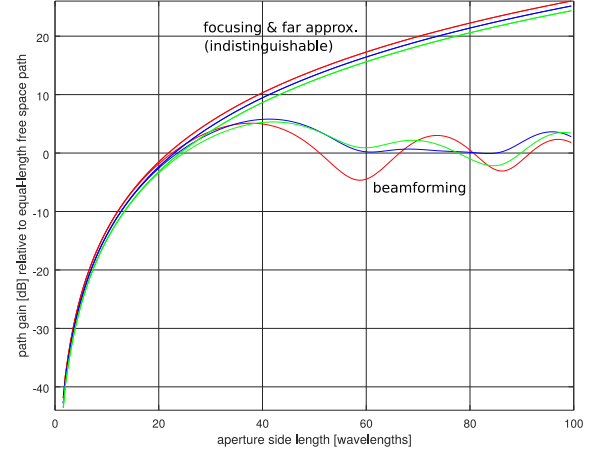


Fig. 3. Path gain relative to the equal-length free space channel for $r_i = r_s = 10^3\lambda$. Curves are shown for $\psi_s = 0^\circ$ (red), 60° (blue), and 75° (green).

for focusing, beamforming, and the far approximation. In this case, focusing and the far approximation remain too close to distinguish. Therefore the far approximation is very good for RIS apertures up to at least $100\lambda \times 100\lambda$ ($N = 10^4$ elements) for distances $\gtrsim 10^3\lambda$. The performance of beamforming, on the other hand, is seen to be limited to within a few dB of 0 dB for aperture side-lengths greater than about 20λ . In this sense, a RIS operating in beamforming mode might be said to be exhibiting performance comparable to that of specular reflection. This is a particularly useful insight: If beamforming is to be used, then there is a maximum useful size for the RIS, and further increases in size will not significantly reduce path loss. If, on the other hand, focusing is used, then further increases in size *do* significantly reduce path loss.

Figure 4 shows the results of the same experiment performed for $r_i = r_s = 10\lambda$. In this scenario, the RIS side-length

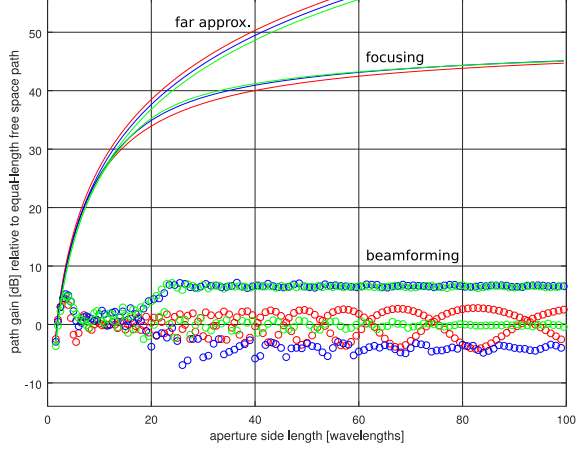


Fig. 4. Path gain relative to the equal-length free space channel for $r_i = r_s = 10\lambda$. Curves are shown for $\psi_s = 0^\circ$ (red), 60° (blue), and 75° (green). Beamforming results are shown as unconnected data points to make clear the rapid variation even when varying the aperture size by the minimum amount; i.e., by one additional row and column of elements per sample.

becomes much larger than the distances to the transmitter and receiver, and so the far approximation is expected to fail. This is observed to be the case, with the results for focusing and the far approximation diverging for side-lengths greater than about r_i (or r_s). Focusing approaches 45 dB normalized path gain for 100λ side-length, compared to 0 ± 6 dB (independent of side length) for beamforming. Thus – as expected – focusing is capable of enormous gain over beamforming when path distances are small relative to aperture side-length.

VI. CONCLUSIONS

This paper presented a physical model for RIS scattering (Equations 8–11) and employed the model to develop a general expression for aggregate path loss (Equation 13). To avoid the need for implementation-specific RIS design parameters, a physically-motivated benchmark element pattern model was proposed (Equations 14–16 with $q = q_0 = 0.285$), for which the broadside gain is about 5 dBi. This pattern has the useful feature that the sum of the broadside effective areas of the elements is equal to the physical area of the RIS when the element spacing is $\lambda/2$. Other RISs can be accurately represented by varying q and the element spacing.

Application of the benchmark element pattern to the far case yields Equation 24, which simplifies to Equation 25 when the b_n 's (controlled magnitudes and phases) are selected for minimum path loss, and further simplifies to Equation 27 if the element spacing is actually $\lambda/2$. We find in that case that the path loss depends only on the physical size of the RIS, and not at all on frequency or dimensions relative to wavelength. It was further shown that this result is consistent with flat plate scattering theory and exhibits $r_i^2 r_s^2$ range dependence regardless of element pattern, element spacing, or scheme for selecting b_n 's.

The far case results are compared to the free space (i.e., no RIS) channel having the same path length, and it is shown

that the path loss of the RIS-enabled channel may be equal to, less than, or greater. This analysis yields a useful guideline (Equation 35) for identifying the RIS physical area required to achieve path loss equal to that of the equal path length free space channel.

The analysis was repeated for the general (i.e., not necessarily far) case. Here it is necessary to distinguish between focusing and beamforming, and it was found that beamforming (but not focusing) exhibits performance within a few dB of specular reflection if the ratio of distance to RIS size is sufficient small. When this is the case, there is an upper limit on the useful size of the RIS (found to be on the order of 20λ for the scenario considered).

Considerations not addressed in this paper include variation in element patterns (specifically, differences between interior and edge elements due to mutual coupling) and polarization. However these issues can be addressed via straightforward modifications of the analysis presented in this paper.

REFERENCES

- [1] E. Basar *et al.*, “Wireless Communications Through Reconfigurable Intelligent Surfaces,” *IEEE Access*, Vol. 7, Sep. 2019, pp. 116753–73.
- [2] W. Saad, M. Bennis & M. Chen, “A Vision of 6G Wireless Systems: Applications, Trends, Technologies, and Open Research Problems,” Jul. 2019. [Online]. Available: arXiv:1902.10265v2. (*IEEE Network in press*)
- [3] Y. Han *et al.*, “Large Intelligent Surface-Assisted Wireless Communication Exploiting Statistical CSI,” *IEEE Trans. Veh. Tech.*, Vol. 68, No. 8, Aug. 2019, pp. 8238–42.
- [4] Q. Wu and R. Zhang, “Towards Smart and Reconfigurable Environment: Intelligent Reflecting Surface Aided Wireless Network,” Jul. 2019. [Online]. Available: arXiv:1905.00152v4. (*IEEE Comm. Mag. in press*)
- [5] C. Liaskos *et al.*, “A New Wireless Communication Paradigm through Software-Controlled Metasurfaces,” *IEEE Comm. Mag.*, Vol. 56, No. 9, Sep. 2018, pp. 162–9.
- [6] Ö. Özdogan, E. Björnson & E. Larsson, “Intelligent Reflecting Surfaces: Physics, Propagation, and Pathloss Modeling,” Oct. 2019. [Online]. Available: arXiv:1911.03359v1.
- [7] W. Tang, *et al.*, “Wireless Communications with Reconfigurable Intelligent Surface: Path Loss Modeling and Experimental Measurement,” Nov. 2019. [Online]. Available: arXiv:1911.05326v1.
- [8] W.L. Stutzman & G.A. Thiele, *Antenna Theory and Design*, 3rd Ed., Wiley, 2012.
- [9] R.F. Harrington, *Time-Harmonic Electromagnetic Fields*, McGraw-Hill, 1961.